Biophysical Journal, Volume *118*

Supplemental Information

The Poisson Ratio of the Cellular Actin Cortex Is Frequency Dependent

Marcel Mokbel, Kamran Hosseini, Sebastian Aland, and Elisabeth Fischer-Friedrich

Supporting material:
The Poisson ratio of the cellular actin cortex is frequency-dependent

M. Mokbel,[1] K. Hosseini,[2,3] S. Aland,[1, a)] and E. Fischer-Friedrich[2, 3, b)]
[1)] *Faculty of Informatics/Mathematics, Hochschule für Technik und Wirtschaft, Dresden, Germany*
[2)] *Cluster of Excellence Physics of Life, Technische Universität Dresden, Dresden, Germany*
[3)] *Biotechnology Center, Technische Universität Dresden, Dresden, Germany*

I. EFFECTIVE COMPRESSION MODULUS OF A THIN POROELASTIC LAYER

In the following, we estimate an effective bulk modulus of a fluid-filled elastic scaffold taking into account fluxes of the fluid relative to the scaffold. We show that poroelastic effects likely affect compressibility of the actin cytoskeleton only for frequencies significantly higher than 10 Hz.
For a poroelastic material consisting of a viscoelastic porous scaffold and an immersing fluid, we have in Cartesian coordinates[1]

$$\epsilon_{ii} = \frac{1}{K}\left(\frac{\sigma_{ii}}{3} + p_H\right), \tag{1}$$

where p_H is the hydrostatic pressure increment in the fluid, K is the bulk modulus of the scaffold material, and σ_{ij} and ϵ_{ij} are the components of the stress and strain tensor of the elastic scaffold, respectively. Using Darcy's law, one obtains[1]

$$\frac{k_{perm}}{\eta}\Delta p_H = \frac{\partial \epsilon_{ii}}{\partial t}, \tag{2}$$

where k_{perm} characterizes the permeability of the scaffold material, η is the viscosity of the immersing fluid and Δ is the Laplace operator. Consider a flat horizontal layer of porous material with thickness t_c. We choose the middle layer of the layer to be at coordinate $z = 0$. Consider that oscillating opposing uniform forces are applied at the top and the bottom of the layer by a porous slab such that a small time-periodic (sinusoidal) compression is achieved. The edges of the layer are clamped such that displacement in x- and y-direction are prohibited. In this case, the trace of the strain tensor is $\epsilon_{ii} = \epsilon_{zz}$. Equivalently, $\sigma_{ii} = \sigma_{zz}$, where σ_{zz} varies time-periodically but is spatially uniform due to the force balance requirement $\partial_z \sigma_{zz} = 0$. According to Eqn. (1) and (2), we have $\epsilon_{zz} = \frac{1}{K}(\frac{\sigma_{zz}}{3} + p_H)$ and $i\omega\epsilon_{zz} = \frac{k_{perm}}{\eta}\partial_z^2 p_H$, where we identified the time-derivative with a multiplication by $i\omega$. We therefore obtain the following partial differential equation in p_H

$$\frac{i\omega}{K}\left(\frac{\sigma_{zz}}{3} + p_H\right) = \frac{k_{perm}}{\eta}\partial_z^2 p_H. \tag{3}$$

A special solution of Eq. (3) is $p_H = -\sigma_{zz}/3$. The general solution of the corrsponding homogeneous equation reads $p_H^h(z) = Ae^{\frac{z}{\lambda}} + Be^{-\frac{z}{\lambda}}$, where $\lambda = \sqrt{\frac{Kk_{perm}}{i\omega\eta}}$. Assuming that the porosity of the confining slabs is significantly larger than the porosity of the poroelastic layer, we impose the boundary conditions[1] $p_H(z = \pm t_c/2) = 0$ and obtain the full solution

$$p_H(t, z) = \frac{\sigma_{zz}(t)}{3}\left(\frac{(e^{\frac{z}{\lambda}} + e^{-\frac{z}{\lambda}})}{(e^{\frac{t_c}{2\lambda}} + e^{-\frac{t_c}{2\lambda}})} - 1\right) \tag{4}$$

For the strain, we find

$$\epsilon_{zz}(t, z) = \frac{\sigma_{zz}}{3K}\frac{(e^{\frac{z}{\lambda}} + e^{-\frac{z}{\lambda}})}{(e^{\frac{t_c}{2\lambda}} + e^{-\frac{t_c}{2\lambda}})} \tag{5}$$

[a)] Electronic mail: Corresponding author: sebastian.aland@htw-dresden.de
[b)] Electronic mail: Corresponding author: elisabeth.fischer-friedrich@tu-dresden.de

Accordingly, we obtain for the displacement component in z-direction

$$u_z(t,z) = \frac{\sigma_{zz}\lambda}{3K}\frac{(e^{\frac{z}{\lambda}} - e^{-\frac{z}{\lambda}})}{(e^{\frac{t_c}{2\lambda}} + e^{-\frac{t_c}{2\lambda}})}, \tag{6}$$

For large λ, the displacement at the boundary $z = t_c/2$ can be rewritten as

$$u_z(z = t/2) = \frac{\sigma_{zz}}{3K\left(1 + \frac{t_c^2}{12\lambda^2}\right)}\frac{t_c}{2} + \mathcal{O}(\frac{1}{\lambda^4}), \tag{7}$$

where $\mathcal{O}$ denotes the Landau symbol. Therefore, we may infer an effective compression modulus of the form

$$K_{eff} = K\left(1 + \frac{t_c^2}{12\lambda^2}\right) = \left(K + \frac{i\omega\eta t_c^2}{12k_{perm}}\right).$$

The absolute value of K_{eff} grows with frequency reflecting a trend to approach an effective incompressibility in the large frequency regime.

In the following, we will give a rough order of magnitude estimate of the dissipative term $\frac{i\omega\eta t_c^2}{12k_{perm}}$ in K_{eff} for parameters of the actin cortex layer in mitotic cells. Based on the Hagen-Poiseuille equation[2], we estimate the permeability of the actin cytoskeleton as $d_{pore}^2/32$, where d_{pore} is the diameter of a cytoskeletal pore which we assume to be $\approx 50\,\mathrm{nm}$ for the mitotic cortex[3]. Furthermore, we estimate the cytoplasmic viscosity η inside the cortical pores to be $\approx 10^{-3}\mathrm{Pa}\cdot\mathrm{s}$ [4]. The length scale t_c is approximated by the previously measured thickness of the cortex ($200\,\mathrm{nm}$) [5]. We thus obtain an estimate of the dissipative (imaginary) term of K_{eff} of the cortex of $\approx 100\,\mathrm{Pa}$ at $f = 10\,\mathrm{Hz}$. This elastic modulus is still more than an order of magnitude lower than the shear modulus of the mitotic cortex at $10\,\mathrm{Hz}$ which can be inferred from[6] to be $\approx 200\,\mathrm{kPa}$. Thus, we expect that the dissipative, imaginary term of K_{eff} gives a small, negligible contribution at frequency $f = 10\,\mathrm{Hz}$ and lower frequencies because $K \gtrsim G$ (provided that $\nu > 0$).

II. INFLUENCE OF INTERNAL VISCOSITY ON CELL MECHANICAL RESPONSE

In the following section, we show that the force response of the liquid interior of a model cell adds $\leq 1\%$ to the effective modulus K of uniaxial compression for cytoplasmic viscosities of up to $1\,\mathrm{Pa}\cdot\mathrm{s}$ and is thus negligible for our study.

In our simulations, we tested the influence of internal cytoplasmic viscosity on the force response of measured cells. To this end, we simulated the time-periodic deformation of model cells, that were constituted by an elastic shell with typical cell parameters and a viscous incompressible (pressurized) interior (Fig. 1). Typical values for the viscosity of the non-cytoskeletal phase of the cytoplasm range between $10^{-3} - 10^{-2}\,\mathrm{Pa}\cdot\mathrm{s}$ [4,7]. From our simulations, we find that the force contribution due to viscous friction generated by cyclic cytoplasmic deformation is negligible up to frequencies of $10\,\mathrm{Hz}$ and viscosities of $1\,\mathrm{Pa}\cdot\mathrm{s}$. There, the calculated effective elastic modulus of the model cell agrees within 1% with the modulus obtained for the case of vanishing internal viscosity (Fig. 1). This finding suggests that cytoplasmic viscosities give a negligible contribution to the mechanical response of cells during our cell-mechanical probing, which is corroborated by earlier experimental findings[6]. At a probing frequency of $10\,\mathrm{Hz}$, we start to see notable changes of the elastic modulus for $\eta = 10\,\mathrm{Pa}\cdot\mathrm{s}$ in simulations (Fig. 1).

III. UNIAXIAL COMPRESSION OF MODEL CELLS AND PHENOMENOLOGICAL LAWS

In the following section, we describe the parametrisation and analysis of model cell compression that were used for generation of the data as presented in the main text, Fig. 2. Finally, we present phenomenological laws that approximate the functional dependencies of effective modulus K and parameter α as found in simulations.

In our study, we performed simulations of a small uniaxial compression step ($\Delta h = 0.5\,\mu\mathrm{m}$) of pressurized elastic shells. Each shell has a thickness of $200\,\mathrm{nm}$, cell volume of $4300\,\mu\mathrm{m}^3$, an area bulk modulus $K_B = 25\,\mathrm{mN/m}$ and an area shear modulus $K_S = 8.3, 10, 15, 20$ or $25\,\mathrm{mN/m}$. For each value of K_S, we simulated compression from an initial reference height of $h_0 = 15, 14, 13, 12, 11$ or $10\,\mu\mathrm{m}$. This was repeated for different values of cortical tension ($\gamma_a = 0.5, 1, 1.5, 2, 2.5$ and $3\,\mathrm{mN/m}$). Therefore, in total $5 \times 6 \times 6 = 180$ simulations have been performed to calibrate the cellular response to uniaxial compression at different mechanical parameters of the cortex. (Furthermore, another 2×180 simulations were performed with equal parameters but deviating bending stiffness testing the influence of changing cortex thickness. There, we assumed i) the absence of bending rigidity or ii) a twofold increased value of

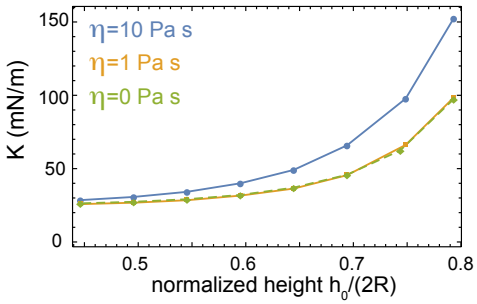

Figure 1. Effective shell moduli calculated from simulations in the presence of a viscous bulk of varying viscosity η. Mechanical parameters of the model cell's shell were $K_B = 25\,\mathrm{mN/m}$, $K_S = 8.33\,\mathrm{mN/m}$, $\gamma_a = 1.5\,\mathrm{mN/m}$, $t = 200\,\mathrm{nm}$. Up to a viscosity of $1\,\mathrm{Pa}\cdot\mathrm{s}$, the influence of the bulk viscosity is negligible. At $\eta = 10\,\mathrm{Pa}\cdot\mathrm{s}$, the bulk viscosity increases the calculated effective modulus of the model cell.

bending rigidity, see Section VI.)
From each simulation, we extracted the force exerted on the elastic shell after compression F_{tot} and calculate the effective elastic modulus of the cortical shell K as described in the main text (see Eqn.(1-4), main text).
We describe the height-dependence of the effective shell elastic modulus as $K(\tilde{h}) \approx K_B(1 + \alpha \exp(\tilde{h}/\lambda))$ (see Eq. 5, main text). In this formula, the coefficient λ was determined from an exponential fit of simulated data by the function $K_B(1+\alpha \exp(\tilde{h}/c))$. We noted, that the fit parameter c varied only slightly in dependence of shell parameters $\tilde{K}_S$ and $\tilde{\gamma}_a$. To spare the characteristic height scale c as a fit parameter for our noisy experimental data, we used henceforth its average value $\lambda = 0.091081$. In turn, we refitted the effective moduli of simulated data by $K_B(1 + \alpha(\tilde{K}_S) \exp(\tilde{h}/\lambda))$ for set values of K_B, K_S and γ_a, providing α as a function of the dimensionless parameters $\tilde{K}_S = K_S/K_B$ and $\tilde{\gamma}_a = \gamma_a/K_B$. For a given value of $\tilde{\gamma}_a$, the dependence of α on $\tilde{K}_S$ is captured by a fit function $C(\tilde{\gamma}_a)\ln[\tilde{K}_S] + D(\tilde{\gamma}_a)$. Finally, the dependence of the fit parameters $C(\tilde{\gamma}_a)$ and $D(\tilde{\gamma}_a)$ on the parameter $\tilde{\gamma}_a$ is captured through a polynomial fit of third degree:

$$C_{fit}(\tilde{\gamma}_a) = (1.09 \cdot 10^{-4} + 1.071 \cdot 10^{-4}\,\tilde{\gamma}_a - 1.54 \cdot 10^{-5}\,\tilde{\gamma}_a^2 + 1.08 \cdot 10^{-6}\,\tilde{\gamma}_a^3),$$
$$D_{fit}(\tilde{\gamma}_a) = (9.418 \cdot 10^{-6} - 5.874 \cdot 10^{-5}\,\tilde{\gamma}_a - 2.157 \cdot 10^{-5}\,\tilde{\gamma}_a^2 + 4.44 \cdot 10^{-6}\,\tilde{\gamma}_a^3).$$

By construction, the resulting function $C_{fit}(\tilde{\gamma}_a)\ln[\tilde{K}_S] + D_{fit}(\tilde{\gamma}_a)$ makes excellent quantitative predictions about the value of α in dependence of $\tilde{\gamma}_a$ and $\tilde{K}_S$ (Fig. 2d, main text).
For simulations with the alternative assumptions of i) twofold bending stiffness and ii) vanishing bending stiffness, we obtain different fit polynomials. For i), we have

$$C_{fit}(\tilde{\gamma}_a) = (1.59 \cdot 10^{-4} + 1.09 \cdot 10^{-4}\,\tilde{\gamma}_a - 1.15 \cdot 10^{-5}\,\tilde{\gamma}_a^2 + 4.4 \cdot 10^{-8}\,\tilde{\gamma}_a^3),$$
$$D_{fit}(\tilde{\gamma}_a) = (-3.09 \cdot 10^{-5} - 5.41 \cdot 10^{-5}\,\tilde{\gamma}_a - 3.68 \cdot 10^{-5}\,\tilde{\gamma}_a^2 + 7.87 \cdot 10^{-6}\,\tilde{\gamma}_a^3).$$

For ii), we find

$$C_{fit}(\tilde{\gamma}_a) = (4.22 \cdot 10^{-5} + 1.5 \cdot 10^{-4}\,\tilde{\gamma}_a - 4.67 \cdot 10^{-5}\,\tilde{\gamma}_a^2 + 6.34 \cdot 10^{-6}\,\tilde{\gamma}_a^3),$$
$$D_{fit}(\tilde{\gamma}_a) = (8.62 \cdot 10^{-5} - 1.65 \cdot 10^{-4}\,\tilde{\gamma}_a + 4.76 \cdot 10^{-5}\,\tilde{\gamma}_a^2 - 8.42 \cdot 10^{-6}\,\tilde{\gamma}_a^3).$$

IV. CELL DEFORMATION SIMULATIONS

Simulations were performed using the finite element (FEM) toolbox AMDiS, developed at the Institute of Scientific Computing TU Dresden[8,9]. We use an axisymmetric Arbitrary Lagrangian Eulerian (ALE) model with incompressible Navier-Stokes equations for the viscous fluid inside the cell, where the two plates and the forces acting on the membrane are implemented as boundary conditions.
We assume the cell to be in a stationary state initially, where elastic parameters have no influence on the force exerted by the cell on the plates. The cell is then compressed by a prescribed sinusoidal decrease of the distance h between the plates, while simultaneously calculating the force exerted on the upper plate.

Using axisymmetry normal to the plates, we can perform calculations on a two dimensional domain describing half of the cell's cross-section. An example image of the simulation domain is shown in Fig. 2. The interior of the cell is denoted by the computational domain Ω which is bounded by the cell cortex/membrane Γ and the symmetry axis. Γ itself is subdivided into the area touching the plates Γ_p and the free surface area Γ_f. During compression a part of the free surface will touch the plate, accordingly Γ_p and Γ_f are time-dependent:

$$\Gamma_p(t) = \{\mathbf{x} = (x_0, x_1) \in \Gamma : x_1 = 0 \vee x_1 = h(t)\}, \qquad \Gamma_f(t) = \Gamma / \Gamma_p(t). \tag{8}$$

The interface curve of Γ for the initial meshes with $h = h_0$ is given by a minimal surface calculated according to equations described in[10].

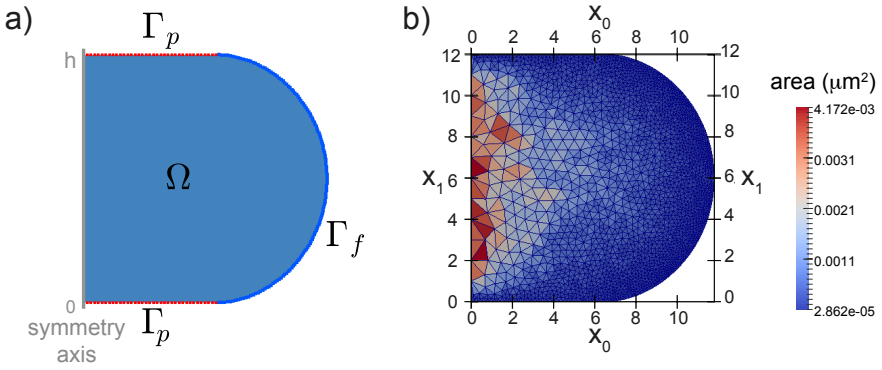

Figure 2. (a) Example image for a simulation domain Ω. The plates here are on the top and bottom sides of the cell with the boundary Γ_p (red dotted line). The free part of the boundary of the cell is Γ_f (blue line). (b) Example image for the mesh for $h_0 = 12\,\mu$m. The color scale indicates the areas of the triangles.

The system is governed by the axisymmetric Navier-Stokes equations[11] together with the surface forces and contact conditions for the plate,

$$\rho\, \partial_t^\bullet \mathbf{v} = \nabla \cdot \mathbf{S} + \frac{\eta}{x_0} \begin{pmatrix} 2\partial_{x_0} v_0 \\ \partial_{x_0} v_1 + \partial_{x_1} v_0 \end{pmatrix} + \frac{2\eta}{(x_0)^2} \begin{pmatrix} v_0 \\ 0 \end{pmatrix}, \qquad \text{in } \Omega \tag{9}$$

$$\nabla \cdot \mathbf{v} + \frac{1}{x_0} v_0 = 0, \qquad \text{in } \Omega \tag{10}$$

$$\mathbf{S} = \eta \left(\nabla \mathbf{v} + \nabla \mathbf{v}^T\right) - p\mathbf{I}, \qquad \text{in } \Omega \tag{11}$$

$$\mathbf{S} \cdot \mathbf{n} = -\frac{\partial E_{\text{tension}}}{\partial \Gamma} - \frac{\partial E_{\text{bend}}}{\partial \Gamma} - \frac{\partial E_{\text{stretch}}}{\partial \Gamma}, \qquad \text{on } \Gamma_f \tag{12}$$

$$[\mathbf{S} \cdot \mathbf{n}]_0 = \left[-\frac{\partial E_{\text{tension}}}{\partial \Gamma} - \frac{\partial E_{\text{bend}}}{\partial \Gamma} - \frac{\partial E_{\text{stretch}}}{\partial \Gamma} \right]_0, \qquad \text{on } \Gamma_p \tag{13}$$

$$v_1 = \delta_{x_1 > 0} \cdot \partial_t h, \qquad \text{on } \Gamma_p \tag{14}$$

$$v_0 = 0, \qquad \text{on } \partial\Omega / \Gamma \tag{15}$$

where ρ is the mass density of cytoplasm, $\partial_t^\bullet \mathbf{v}$ denotes the material derivative of the velocity field $\mathbf{v} = (v_0, v_1)$ of the cytoplasmic fluid, p is the pressure field, η the viscosity, $\mathbf{n}$ the outer unit normal of the domain on Γ, and $\mathbf{S}$ is the bulk stress measured in N/m^2. The first variation of the interfacial energies with respect to changes in Γ yields the interfacial forces. We have[12]

$$\frac{\partial E_{\text{tension}}}{\partial \Gamma} = -2\gamma_a H \mathbf{n}, \quad \frac{\partial E_{\text{bend}}}{\partial \Gamma} = B \left(2\Delta \left(H - H_0\right) + 4\left(2H^2 - K_G\right)\left(H - H_0\right) - 4H\left(H - H_0\right)^2\right) \mathbf{n}, \tag{16}$$

where γ_a is the active surface tension, B is the bending stiffness of the cell cortex, H the mean curvature, H_0 the mean curvature in the initial state, and K_G the gaussian curvature, respectively. Formulas for the calculation of the curvatures of an axisymmetric surface grid can be found in[13].
The formula for the elastic force involves the two principal stretches λ_1 and λ_2, that describe the relative change of the surface length in lateral and rotational direction, respectively:

$$\lambda_1 = \frac{\mathrm{d}s}{\mathrm{d}s_{|t=0}}, \lambda_2 = \frac{x_0}{x_{0|t=0}}, \tag{17}$$

where s is the arc length, x_0 the distance to the symmetry axis, and $s_{|t=0}$ and $x_{0|t=0}$ are the corresponding quantities at the same material point in the initial state. With this, we can write[12]

$$\frac{\partial E_{\text{stretch}}}{\partial \Gamma} = (2H\,\mathbf{n} - \nabla_\Gamma)\left[(K_B + K_S)\,(\lambda_1 - 1) + (K_B - K_S)\,(\lambda_2 - 1)\right] - 2K_S\,(\lambda_1 - \lambda_2)\,\frac{1}{x_0}\begin{pmatrix}1\\0\end{pmatrix}. \tag{18}$$

The discretization is done by an ALE method, where grid points at the cell surface Γ are moved with the velocity $\mathbf{v}$. Interior grid points in Ω are displaced by a harmonic field $\mathbf{w}$ calculated in every time step:

$$\begin{aligned} \Delta \mathbf{w} &= 0, && \text{in } \Omega \\ \mathbf{w} &= \tau \mathbf{v}, && \text{on } \partial\Omega \end{aligned} \tag{19}$$

where τ is the time step size. Whenever a grid point of the free boundary, $\mathbf{x} = (x_0, x_1) \in \Gamma_f$, reaches the lower or upper plate, $x_1 \leq 0$ or $x_1 \geq h$, it is moved exactly onto the plate, i.e. $x_1 = 0$ or $x_1 = h$, respectively, and we mark the point as a member of the discrete points set of Γ_p instead of Γ_f.
The position (and velocity) of the moving plate are prescribed by a cosine function

$$h(t) = h_0 - \frac{\Delta h}{2}\left[1 - \cos\left(2\pi f \cdot (t - t_0)\right)\right], \tag{20}$$

where f is the oscillation frequency. The compression starts at $t = t_0$ and ends at $\tilde{t} = 1/(2f) + t_0$, where maximum compression is reached. For $t > \tilde{t}$, we keep the cell in the compressed state, $h(t) = h_0 - \Delta h$.
The force, exerted on the upper plate, is calculated in every time step using

$$F_{\text{plate}} = 2\pi \int_\Gamma a(x_0, x_1) \cdot x_0 \cdot \left[\mathbf{S} \cdot \mathbf{n}\right]_1 \, \mathrm{d}\Gamma\,. \tag{21}$$

where the factor $2\pi x_0$ emerges due to axisymmetry, a: $\Gamma \to \mathbb{R}$ is the piecewise linear extension of an indicator function for the upper plate:

$$a(x_0, x_1) = \begin{cases} 1 & \text{if} \quad x_1 \geq h \\ 0 & \text{else}\,. \end{cases} \tag{22}$$

After compression, i.e. at height $h_0 - \Delta h$, we have $F_{plate} = F_{tot}$, cf. Eq. (2) main text.
As shown in see Sec. II, we found that the contribution of interior viscosity to the force response is negligible. To simulate the process without interior viscosity, one can take advantage of some simplifications. In this case, we do not need a 2D mesh representing half of the cell's cross section but only a 1D mesh representing the membrane Γ in Fig. 2(a). Accordingly, the Navier-Stokes equations (9)-(13) are replaced by a set of equations that only determine the velocity field on the surface Γ,

$$\mathbf{v} = \mu\left[-\frac{\partial E_{\text{tension}}}{\partial \Gamma} - \frac{\partial E_{\text{bend}}}{\partial \Gamma} - \frac{\partial E_{\text{stretch}}}{\partial \Gamma} - p_c(V - V_0)\,\mathbf{n}\right], \qquad \text{on } \Gamma_f \tag{23}$$

$$\mathbf{v} = \begin{pmatrix} \mu\left[-\frac{\partial E_{\text{tension}}}{\partial \Gamma} - \frac{\partial E_{\text{bend}}}{\partial \Gamma} - \frac{\partial E_{\text{stretch}}}{\partial \Gamma}\right]_0 \\ \delta_{x_1>0} \cdot \partial_t h \end{pmatrix}, \qquad \text{on } \Gamma_p \tag{24}$$

where V is the (3D) volume of the cell, V_0 is the volume in the initial state and p_c is a large constant to provide the pressure to ensure volume conservation. In the absence of viscosity, the (inverse) coefficient of friction μ controls the dynamics and must be chosen large enough to keep the system in an equilibrated state. Here we use $\mu = 1.25 \cdot 10^{-7}\,\mathrm{m^2 s/kg}$. We verified numerically that this choice relaxes surface forces from elastic deformation on a time scale much faster than the period of the prescribed height oscillations. In particular μ is large enough that simulation results are invariant to a further increase in μ. Cell volume is conserved by a penalty approach. Being multiplied by the normal vector, the term $p_c(V - V_0)$ plays the role of a pressure. For large p_c this term dominates equation (23) to highest order which leads to $V = V_0$. We have chosen $p_c = 1.2 \cdot 10^5\,\mathrm{N/m^5}$ which is large enough to ensure the relative change in volume is less than 0.01% for all times.
The interfacial forces are implemented explicitly, i.e. curvatures and principal stretches of the configuration in the previous time step are used to calculate the force in the new time step. Therefore, the system is quite restrictive to time step sizes. For the simulations with interior flow, a time step of 0.5μs is used. Hence, for an oscillation frequency of 10Hz we need ≈ 200.000 time steps to simulate a full period of 0.1 s. The initial mesh is shown in Fig. 2(b) for $h_0 = 12\,\mu$m. A fine mesh at the membrane is necessary to produce highly accurate results for the membrane forces. Hence, the triangle sizes amount from approximately $0.003\,\mu\mathrm{m}^2$ at the interface to $0.4\,\mu\mathrm{m}^2$ around the cell center.

V. SCATTER OF ESTIMATED POISSON RATIOS AT DIFFERENT FREQUENCIES

In this section, we present histograms of experimentally measured values $\tilde{K}_S = K_S/K_B$ as well as associated Poisson ratios for all frequencies measured (Fig. 3(a,b)). Furthermore, we discuss fitting of respective distributions and sources of data scatter.
Histograms of $\tilde{K}_S$ are shown in have been fitted with the lognormal distribution of maximum likelihood (Fig. 3(a)). Histograms of Poisson ratio ν are plotted with the distribution induced by the lognormal distribution of $\tilde{K}_S$ (Fig. 3(b)). This induced distribution is calculated by the functional relationship $\nu = (1 - \tilde{K}_S)/(1 + \tilde{K}_S)$.
In Fig. 3(c), we analyzed simulated data in the same way as experimental data, however not using the exact values for cell volume and cell height. Instead, we drew the values of cell volume and cell height from a Gaussian distribution with correct mean value and a standard deviation that matches our error estimate for cell volume and cell height (7.5% and 0.5 μm, respectively). We chose $N = 55$, similar to sample numbers measured in the experiments. The resulting scatter in estimated Poisson ratios is shown in Fig. 3(c), where the horizontal lines indicate median, 25th percentile and 75th percentile. While the median is close to actual values of the Poisson ratio, the resulting scatter is substantial, in particular for $\nu = 0.25$. We conclude that the large scatter of Poisson ratios observed in our experimental data does not exclusively result from mechanical variations between cells but stems to a substantial amount from experimental uncertainties.

VI. INFLUENCE OF CORTICAL THICKNESS AND BENDING STIFFNESS VARIATIONS ON POISSON RATIO ESTIMATES

Cortical thickness in mitotic HeLa cells has previously been estimated to be $\approx 200\,\mathrm{nm}$[5]. However, cells exhibit cell-cell variations in cortical thickness and thus variations in cortical bending stiffness which will contribute to scatter of Poisson ratio estimates in our analysis. In order to examine the influence of cell-cell variations in cortical bending stiffness, we repeated our simulations of cell deformation with i) twofold increased bending stiffness (corresponding to $\approx 40\%$ relative increase in cortex stiffness) and ii) vanishing bending stiffness of the cortical shell. Using these alternative simulations to calibrate cell mechanical response, we reanalyzed our data. Corresponding alternative Poisson ratio estimates are presented in Fig. 4(b) and (c) where results of the original analysis from Fig. 4(c), main text, are depicted again in Fig. 4(a) for direct comparison. We see that i) the assumption of higher bending stiffnesses of the cortex would lead to consistently higher Poisson ratio estimates for cortical shells. Furthermore, we see that ii) assuming vanishing bending stiffness would consistently lead to lower Poisson ratio estimates of cortical shells. In both cases, the change in Poisson ratio estimates is particularly striking for Poisson ratio values substantially below 0.5. In summary, we conclude that i) an underestimation of cortical bending stiffness in our analysis of experimental data would lead to a consistent underestimation of cortical Poisson ratios, while ii) an overestimation of cortical bending stiffness in our analysis would lead to a consistent overestimation of cortical Poisson ratio in particular if cortical Poisson ratio values are substantially below 0.5. Finally, independent of a possible under- or overestimation of absolute values of the Poisson ratio, we find in all cases a significant trend of Poisson ratio increase with decreasing frequency.

VII. THE TWO-DIMENSIONAL POISSON RATIO OF A THIN SHELL

In the following, we show that the two-dimensional Poisson ratio ν_{2D} of a thin shell, made up of a thin layer of an isotropic material, equals the respective three-dimensional Poisson ratio ν of the material.
For the surface energy density of stretching of a thin shell, one obtains in complete analogy to the three-dimensional case[16]

$$F = K_S(\epsilon_{ij} - \frac{\delta_{ij}}{2}\epsilon_{ll})^2 + \frac{1}{2}K_B(\epsilon_{ll})^2, \tag{25}$$

where K_B and K_S are the area bulk modulus and the area shear modulus of the shell and $\epsilon_{ij}, (i, j = 1, 2)$ are in-plane coefficients of the strain tensor. The corresponding stress-strain relationship reads

$$\sigma_{ij} = 2K_S(\epsilon_{ij} - \frac{\delta_{ij}}{2}\epsilon_{ll}) + K_B\delta_{ij}\epsilon_{ll}. \tag{26}$$

Correspondingly, the strain can be written as

$$\epsilon_{ij} = \frac{1}{2K_S}(\sigma_{ij} - \frac{\delta_{ij}}{2}\sigma_{ll}) + \frac{1}{4K_B}\delta_{ij}\sigma_{ll}. \tag{27}$$

We will now determine the expression of the two-dimensional Poisson ratio of a thin shell as a function of K_B and K_S. To this end, we consider the special case of a thin, flat, square-shaped patch of a shell subject to a uniform in-plane stretch through opposite forces acting at the top and bottom edge and with free side edges. Correspondingly, the only non-vanishing stress component is σ_{yy}. According to Eq. 27, the strain tensor is given as

$$\boldsymbol{\epsilon} = \frac{1}{2K_S}\begin{pmatrix} \frac{-\sigma_{yy}}{2} & 0 \\ 0 & \frac{\sigma_{yy}}{2} \end{pmatrix} + \frac{1}{4K_B}\begin{pmatrix} \sigma_{yy} & 0 \\ 0 & \sigma_{yy} \end{pmatrix}. \tag{28}$$

The two-dimensional Poisson ratio ν_{2D} is defined as the ratio $\nu_{2D} = -\epsilon_{xx}/\epsilon_{yy}$. With the above relation (28), this equates to $\nu_{2D} = (K_B - K_S)/(K_B + K_S)$. Using the definitions $K_B = t_c G(1+\nu)/(1-\nu)$ and $K_S = t_c G$ for an isotropic shell material with shear modulus G and Poisson ratio ν, we obtain $\nu_{2D} = \nu$. If the constraint of isotropy is released, the two-dimensional Poisson ratio may adopt values in the range $[-1, 1]$.

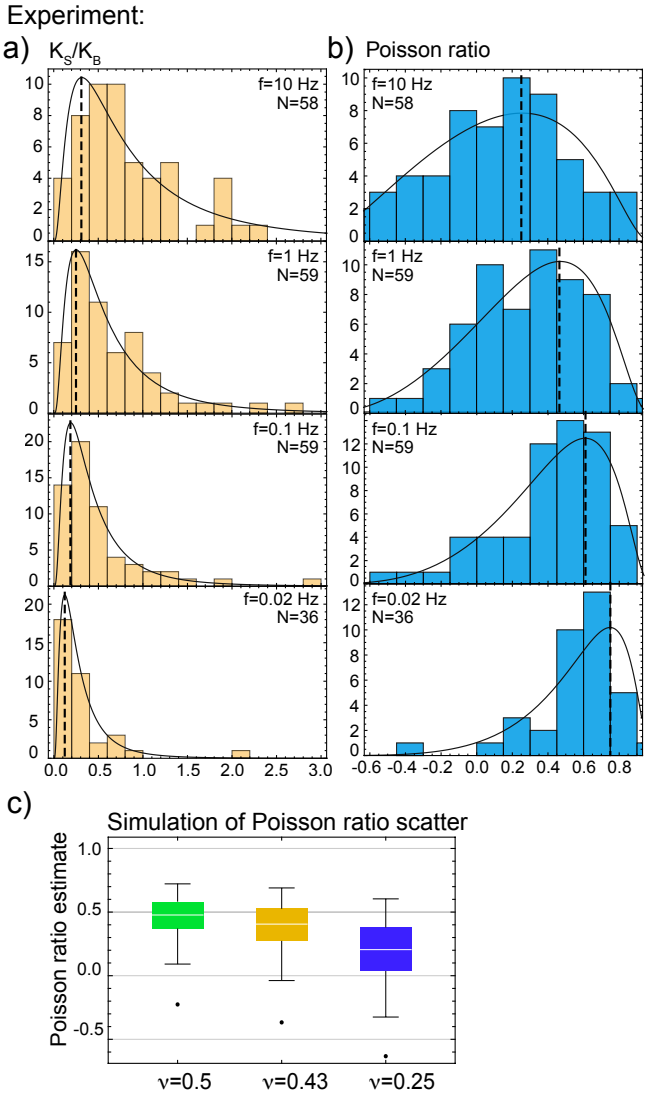

Figure 3. a,b) Results of the analysis of experimental data. a) Histograms of estimated values for the ratio between area shear modulus and area bulk modulus $\tilde{K}_S = K_S/K_B$ with fitted lognormal distributions (logarithmic mean and standard deviation: f=10 Hz, $\mu = -0.31, \sigma = 0.92$; f=1 Hz, $\mu = -0.7, \sigma = 0.82$; f=0.1 Hz, $\mu = -1.03, \sigma = 0.8$; f=0.02 Hz, $\mu = -1.5, \sigma = 0.8$). b) Histograms of estimated Poisson ratios with induced distributions. c) Poisson ratio estimates for simulated data including fake errors of cell volume and cell height. Green data set, $\nu = 0.5$: median: 0.48, IQR: 0.21; orange data set, $\nu = 0.43$: median: 0.41, IQR: 0.25; blue data set, $\nu = 0.25$: median: 0.20, IQR: 0.34, where IQR is the interquartile range, i.e. the distance between 25th and 75th percentile. The sample size was N=55, each, and therefore similar to our experimental sample sizes.

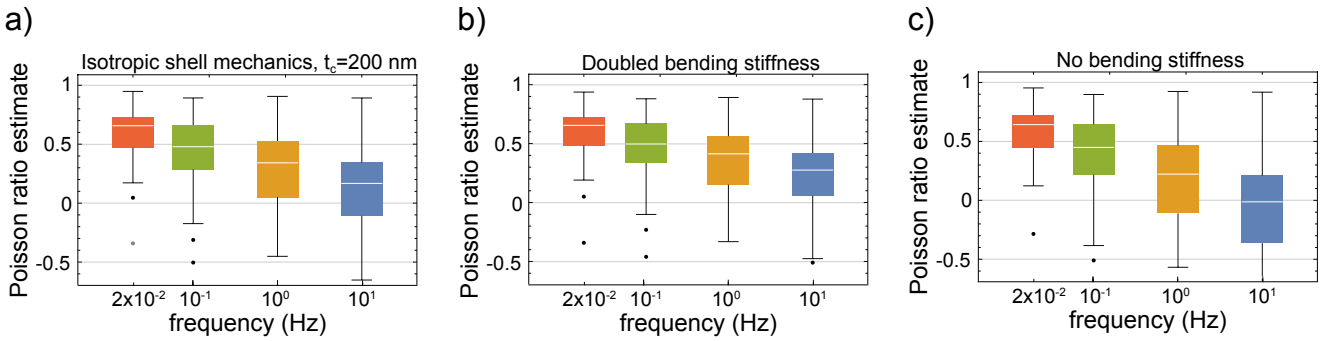

Figure 4. Poisson ratio estimates of the mitotic cortex of HeLa cells using different assumptions on cortical bending stiffness in our analysis (sample sizes from left to right: N=36, N=59, N=59, N=58). a) Estimated Poisson ratios using the assumption of an isotropic cortex with thickness of 200 nm as printed in Fig. 3f, main text. From left to right, median values: 0.66, 0.48, 0.34, 0.17, IQR: 0.26, 0.38, 0.48, 0.45. b) Estimated Poisson ratios using twofold bending stiffness as compared to the analysis in the main text. From left to right, median values: 0.65, 0.5, 0.41, 0.28, IQR: 0.24, 0.33, 0.41, 0.36. c) Estimated Poisson ratios using vanishing bending stiffness. From left to right, median values: 0.64, 0.45, 0.22, -0.013, IQR: 0.3, 0.43, 0.58, 0.57.

REFERENCES

[1]Biot, M. A., and D. G. Willis, 1957. The Theory of Consolidation. 24:594–601.
[2]Granger, R. A., 2012. Fluid Mechanics. Courier Corporation. Google-Books-ID: VWG8AQAAQBAJ.
[3]Charras, G. T., C.-K. Hu, M. Coughlin, and T. J. Mitchison, 2006. Reassembly of contractile actin cortex in cell blebs. 175:477–490.
[4]Kalwarczyk, T., N. Ziębacz, A. Bielejewska, E. Zaboklicka, K. Koynov, J. Szymański, A. Wilk, A. Patkowski, J. Gapiński, H.-J. Butt, and R. Hołyst, 2011. Comparative Analysis of Viscosity of Complex Liquids and Cytoplasm of Mammalian Cells at the Nanoscale. 11:2157–2163.
[5]Clark, A. G., K. Dierkes, and E. K. Paluch, 2013. Monitoring Actin Cortex Thickness in Live Cells. 105:570–580.
[6]Fischer-Friedrich, E., Y. Toyoda, C. J. Cattin, D. J. Müller, A. A. Hyman, and F. Jülicher, 2016. Rheology of the Active Cell Cortex in Mitosis. 111:589–600.
[7]Valentine, M. T., Z. E. Perlman, T. J. Mitchison, and D. A. Weitz, 2005. Mechanical Properties of Xenopus Egg Cytoplasmic Extracts. 88:680–689.
[8]Witkowski, T., S. Ling, S. Praetorius, and A. Voigt, 2015. Software concepts and numerical algorithms for a scalable adaptive parallel finite element method. 41:1145–1177.
[9]Mokbel, M., and S. Aland. An ALE method for simulations of axisymmetric elastic surfaces in flow. .
[10]Fischer-Friedrich, E., A. A. Hyman, F. Jülicher, D. J. Müller, and J. Helenius, 2014. Quantification of surface tension and internal pressure generated by single mitotic cells. 4:6213.
[11]Mokbel, D., H. Abels, and S. Aland, 2018. A phase-field model for fluid-structure interaction. 372:823–840.
[12]Mokbel, M., D. Mokbel, A. Mietke, N. Traber, S. Girardo, O. Otto, J. Guck, and S. Aland, 2017. Numerical simulation of real-time deformability cytometry to extract cell mechanical properties. 3:2962–2973.
[13]Hu, W.-F., Y. Kim, and M.-C. Lai, 2014. An immersed boundary method for simulating the dynamics of three-dimensional axisymmetric vesicles in Navier–Stokes flows. 257:670–686.
[14]Skoufias, D. A., S. DeBonis, Y. Saoudi, L. Lebeau, I. Crevel, R. Cross, R. H. Wade, D. Hackney, and F. Kozielski, 2006. S-Trityl-L-cysteine is a reversible, tight binding inhibitor of the human kinesin Eg5 that specifically blocks mitotic progression. 281:17559–17569.
[15]Stewart, M. P., A. Hodel, A. Spielhofer, C. J. Cattin, D. J. Müller, and J. Helenius, 2013. Wedged AFM-cantilevers for parallel plate cell mechanics. 59:186–194.
[16]Landau, L., and E. Lifshitz, 1986. Theory of Elasticity. Elsevier Ltd., 3rd edition.